Structural transitions in holographic polymer-dispersed liquid crystals

I. Drevenšek-Olenik,[1,2] M. Jazbinšek,[3] M. E. Sousa,[4] A. K. Fontecchio,[4] G. P. Crawford,[4] and M. Čopič[1,2]
[1]*Faculty of Mathematics and Physics, University of Ljubljana, Jadranska 19, SI 1001 Ljubljana, Slovenia*
[2]*J. Stefan Institute, Jamova 39, SI 1001 Ljubljana, Slovenia*
[3]*Swiss Federal Institute of Technology, Nonlinear Optics Laboratory, CH-8093 Zurich, Switzerland*
[4]*Division of Engineering and Department of Physics, Brown University, 182 Hope Street, Providence, Rhode Island 02912, USA*
(Received 12 January 2004; published 18 May 2004)

Dynamic light scattering was used to analyze the structural and dynamic properties of nematic director field within liquid crystal domains formed in holographic polymer-dispersed liquid crystal transmission gratings. Samples prepared from two different types of prepolymer mixture: one curable with visible (VIS) and another curable with UV light were investigated. In both formulations a critical slowing down of thermal director fluctuations, signifying the second-order structural transition of the nematic director field was observed in the vicinity of some critical external electric field as well as close to some critical temperature. For VIS samples also the size and the shape of phase separated droplets and viscoelastic and surface anchoring parameters of the liquid crystalline (LC) material forming the droplets were deduced. The viscoelastic constants were found to significantly deviate from the viscoelastic parameters of the pure LC mixture.

DOI: 10.1103/PhysRevE.69.051703 PACS number(s): 61.30.Pq, 64.70.Md, 42.25.Fx, 42.70.Ln

I. INTRODUCTION

The transformation of data storage, processing, and communication systems from purely electronic devices to hybrid and photonic units is key to the future development of information technology. An important part of these efforts is research on new optical materials for holographic optical elements. Photopolymers are presently the subject of extensive investigations for potential use in holographic recording, as they possess a broad diversity of physical and optical properties and ability to record precise microscopic patterns [1]. Liquid crystals (LC) with their extremely large anisotropies of dielectric and optical properties are, on the other hand, well known electro-optic materials conventionally used for information display devices [2]. A combination of these two attractive features, i.e., liquid crystallinity and photopolymerizability, in various composite media opens up a versatile approach in generating holographic structures for advanced photonic devices.

During the last decade holographic gratings formed from mixtures of photosensitive substances and liquid crystalline compounds in various ratios were investigated for a number of applications [3,4]. These media, commonly referred to as holographic polymer-dispersed liquid crystals (H-PDLC), utilize the photopolymerization induced phase separation in which liquid crystalline material predominantly congregates in dark regions of the optical interference pattern [5,6]. As a result holographic gratings with extremely high-refractive-index contrast are formed. In addition, the diffraction efficiency of these gratings is electrically switchable; the application of an electric field results in reorientation of the nematic director field within the LC domains and consequently the refractive-index mismatch between the LC regions and the polymer network is modified [7]. These features make H-PDLCs very promising media for potential applications in devices such as switchable optical resonators [8,10], diffraction lenses with switchable focus [11,12], optical interconnects [13], and image capture elements [14], as well as for various kinds of reflective display devices [15].

Investigations by scanning electron microscopy (SEM) show that, depending on the composition of the mixture, kinetics of the phase separation process, and the periodicity of the optical pattern, H-PDLCs exhibit a wide range of morphologies: from a well defined stack of alternating planes of LC rich regions (in the form of LC droplets or LC channels embedded in a polymer matrix) separated by layers of a pure polymer up to a three-dimensional (3D) interconnected porous network that hardly reveals any noticeable spatial periodicity [16–24]. These morphological details strongly affect the diffractive properties as well as the switching characteristics of the H-PDLC elements; therefore, a correlation between the structural morphology and optical response of the system is an important problem that needs to be solved in order to optimize the medium for a specific application.

Due to the high birefringence of the LC domains the diffraction efficiency of H-PDLCs strongly depends on the polarization state of the incident light and is usually much larger for polarization perpendicular to the LC rich planes (*p* polarization) than for polarization along the LC rich planes (*s* polarization) (see Fig. 1) [21,25–29]. For structures with a droplet morphology this property is presumably related to the elongated shape of the LC droplets, which in combination with appropriate surface anchoring leads to the nematic director field with preferred direction perpendicular to the holographic planes [5,30,31]. For structures exhibiting nondroplet morphologies, the alignment of LC is attributed to a scaffolding effect of the polymer network [21]. Application of an external electric field and/or modifications of the sample temperature usually cause large variations of the diffraction efficiency. In many cases with increasing field amplitude or temperature the diffraction efficiency for *s* polarization becomes larger than for *p* polarization [27,32]. This feature indicates the appearance of a structural transition of the nematic director field within the LC rich regions.

To verify the presence of the structural transition and gain more insight into the related molecular reorientation pro-

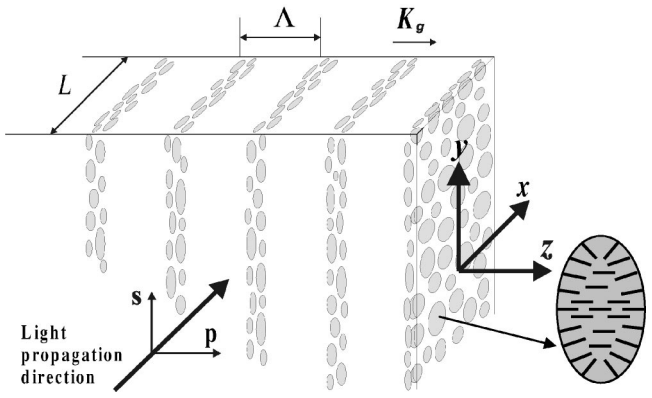

FIG. 1. Schematic drawing of the H-PDLC transmission gratings of thickness L and grating spacing Λ. Droplet planes are perpendicular to the grating wave vector $\mathbf{K}_g$, while average nematic director field within the droplets is parallel to $\mathbf{K}_g$. The directions of *s* and *p* polarizations of incident optical beam are also denoted.

cesses we performed a dynamic light scattering (DLS) study of the thermal director fluctuations in various kinds of H-PDLC transmission gratings as a function of the temperature and applied voltage. The main goal of this work was to observe a softening of the normal mode of fluctuations associated with the transition. However, as the relaxation time of this mode essentially determines the switching characteristics of the gratings, its behavior is important also for potential applications. In addition to this, DLS measurements provide the values of viscoelastic coefficients of the LC material phase separated from the polymer network, which are found to be considerably different from those of a pure LC mixture. Although these data, together with surface anchoring energy coefficients, are a prerequisite to properly explain the dynamic response of the gratings, their dependence on the grating formation procedure has been largely ignored.

II. EXPERIMENT

Different mixtures of commercially available constituents were used to form the transmission gratings. We denote the ones reported in this paper as VIS (visible), UV-A, and UV-B (Table I). There are many variations of these mixtures which can be found in the literature [3,5,7,16–18,23,24]. The VIS mixtures were cured by visible ($\lambda = 532$ nm) and the UV mixtures by UV laser irradiation ($\lambda = 351$ nm) A drop of the prepolymer mixture was placed between two indium tin oxide (ITO)-coated glass substrates separated by 5 μm glass spacers to set the thickness L (Fig. 1). The glass plates have an antireflection coated surface, and the ITO is treated with a layer of index matching coating to avoid spurious reflections during exposure. Photopolymerization was activated by exposing the sample to two interfering laser beams which intersected symmetrically with respect to the sample normal, so that the resulting grating had the grating wave vector $\mathbf{K}_g$ parallel to the sample surfaces (Fig. 1). The pitch of the grating Λ was 0.78 μm for VIS and 1 μm for UV samples. The recording lasted for 30 s with a light intensity of $\approx$150 mW (in each beam) for VIS and 22 mW for UV samples. After recording all the gratings were postcured for 2 min under a broadband UV lamp to stabilize any unreacted

TABLE I. Compositions of the prepolymer emulsions used to prepare our samples.

Label	Constituents
VIS	32.4% BL038 nematic LC[a]
	22.5% aliphatic urethane acrylate oligomer 4866[b]
	22.5%aliphatic urethane acrylate oligomer 8301[b]
	12.6% photoinitiator Rose Bengal, coinitiator
	N-Phenylglycine and chain terminator *N*-Vinyl pyrrolidinone[c]
	10% surfactant S-271 POE sorbitan monooleate[d]
UV-A	55% TL203 nematic LC[a]
	33.5% PN393 mixture of acrylated monomers and oligomers with photoinitiator[a]
	11.5% 1,1,1,3,3,3-Hexafluoroisopropyl acrylate (HFIPA)[c]
UV-B	50% TL205 nematic LC[a]
	24% 2-ethylhexyl acrylate (EHA)[c]
	4.5% aliphatic urethane acrylate oligomer 8301[b]
	1.5% trimethylolpropanetriacrylate (TMPTA)[c]
	20% 1,1,1,3,3,3-Hexafluoroisopropyl acrylate (HFIPA)[c]

[a]EM industries.
[b]Ebecryl (Radcure).
[c]Sigma-Aldrich.
[d]Chem Service.

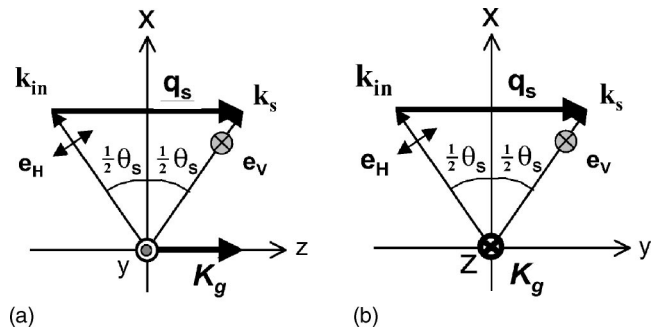

FIG. 2. Illustration of the two orthogonal experimental geometries used in our DLS experiments: (a) $\mathbf{q_s} \| \mathbf{K}_g$, (b) $\mathbf{q_s} \perp \mathbf{K}_g$.

functional groups from further photoreactions. The temperature of the samples was regulated by using an INSTEC microscope hot stage. The effects of external electric field were monitored by applying a 10 kHz square-wave voltage to the ITO electrodes.

DLS measurements were performed using an ALV 5000 digital correlator that enables measurements in the range of $10^{-8}-10^{3}$ s and a He-Ne laser ($P=25$ mW, $\lambda=632.8$ nm) as a light source. The normalized intensity autocorrelation function $g^{(2)}(t)=\langle I_s(0)I_s(t)\rangle/\langle I_s(t)\rangle^2$ of the scattered light was detected. Polarization of the incident laser beam was parallel and polarization of the scattered light was perpendicular to the scattering plane, i.e., the so-called HV scattering geometry was used [33]. For each scattering angle the sample was rotated so that the scattering wave vector $\mathbf{q_s}$ was parallel to the glass substrates and was either parallel to the grating wave vector $\mathbf{K}_g$ or perpendicular it (Figs. 1 and 2). If we neglect small corrections due to birefringence, in such an arrangement the magnitude of $\mathbf{q_s}$ is given by $q_s=(4\pi/\lambda)\sin(\theta_s/2)$, where λ is optical wavelength and θ_s the scattering angle measured in air.

Due to the presence of strong elastic scattering acting as a local oscillator at all scattering angles, the measurements were performed in the heterodyne detection regime in which the normalized field correlation function of the scattered light $g^{(1)}(t)=\langle \mathbf{E}_s^*(0)\mathbf{E}_s(t)\rangle/\langle \mathbf{E}_s^*(t)\mathbf{E}_s(t)\rangle$ is related to $g^{(2)}(t)$ by [33]

$$g^{(2)}(t) = 1 + 2a \ \mathrm{Re}\ g^{(1)}(t), \tag{1}$$

where a is determined by the ratio between inelastic and elastic light scattering intensities. In our experiments a was in the range of 10^{-3}. The field correlation function is associated with the dynamic structure factor of the material

$$S(\mathbf{q_s},t) = \frac{1}{v^2}\int_v \int_v [\langle \delta\varepsilon_{ij}(\mathbf{r},0)\delta\varepsilon_{ij}(\mathbf{r}',t)\rangle^2] e^{i\mathbf{q_s}\cdot(\mathbf{r}-\mathbf{r}')} d^3r d^3r', \tag{2}$$

which is related to $g^{(1)}(t)$ as

$$g^{(1)}(\mathbf{q_s},t) = S(\mathbf{q_s},t)/S(\mathbf{q_s},0), \tag{3}$$

where $\delta\varepsilon_{ij}$ with $i,j=$V, H is a projection of the fluctuation part of the optical dielectric tensor on the polarizations of the incoming and the scattered beam, respectively, while $\langle\ \rangle$ denotes time averaging and v the scattering volume.

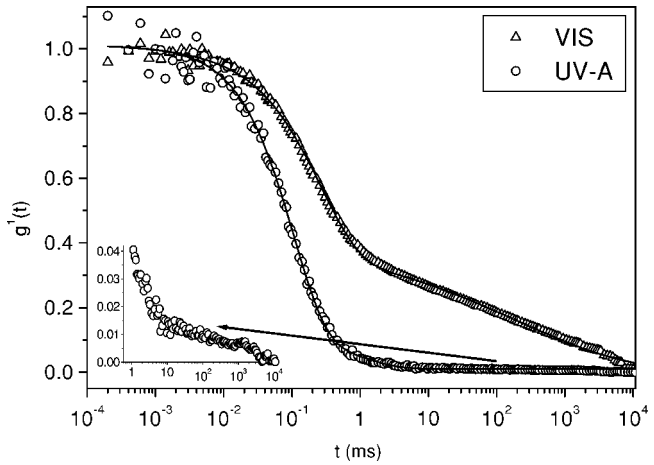

FIG. 3. First-order autocorrelation functions of scattered light detected in VIS and in UV-A samples at small scattering angles at room temperature. Solid lines are fits to Eq. (4).

For dynamic response of a purely dissipative type which is characteristic of thermal director fluctuations of liquid crystals $S(\mathbf{q_s},t)$ can be expressed as [34]

$$S(\mathbf{q_s},t) = \sum_l A_l e^{-(t/\tau_l)^{\beta_l}}, \tag{4}$$

where A_l is the amplitude and τ_l the relaxation time of the lth dynamic mode. The parameter β_l (known also as Kohlrausch-Williams-Watts parameter), which is in the range of $0<\beta_l<1$, characterizes a deviation of the mode from an exponential decay. Its value decreases by increasing polydispersity of the intrinsic response processes of the system. Very broad distributions of dynamic response times are typical for glass and gel forming materials [35].

Diffraction efficiency η_d of the gratings at 632.8 nm was measured by irradiating the sample with the laser beam at Bragg angle. Polarization of the incident beam was set to be either p or s (Fig. 1). Since a significant part of the input beam is reflected and scattered, the diffraction efficiency was calculated as a ratio between the intensity of the first-order diffracted beam and the sum of diffracted and transmitted beam intensities.

III. RESULTS AND DISCUSSION

A. General properties of orientational fluctuations in H-PDLCs

Figure 3 shows two typical autocorrelation functions $g^{(1)}(t)$ measured at room temperature. For all types of the mixtures two dynamic modes are observed: a fast nearly exponential mode with a relaxation time τ_f in the range of 10^{-3} s, and a slow remarkably nonexponential mode with τ_s in the range of $10-10^3$ s and β_s in the interval of $0.2-0.5$. In the VIS samples the amplitudes of both modes are nearly identical, while in the UV samples, especially in the UV-A mixtures, the slow mode is much less pronounced (see inset of Fig. 3). In all samples the relative amplitude of the slow

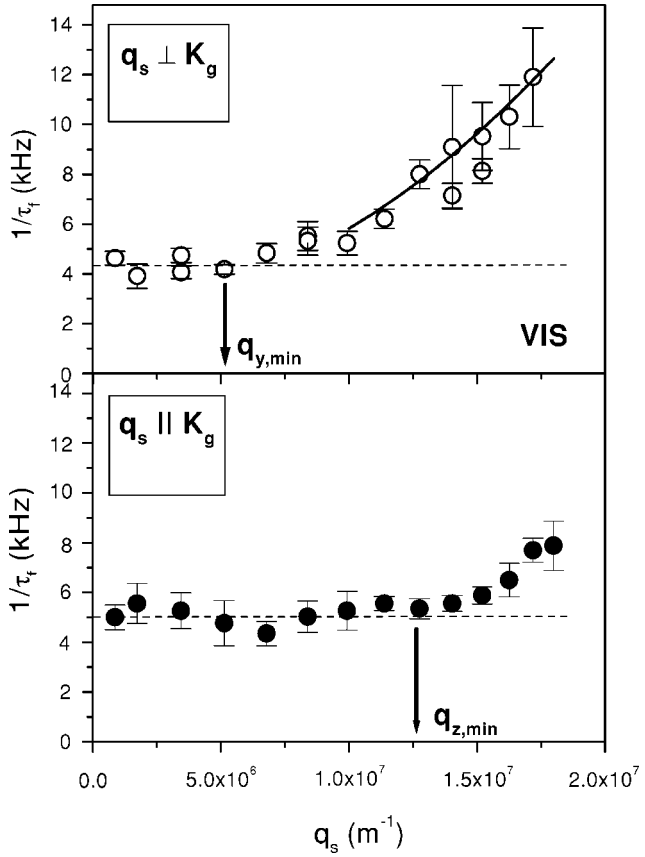

FIG. 4. Dispersion relation of the fast DLS mode measured in VIS sample at room temperature. Solid line is a fit to Eq. (11). Vertical arrows indicate starting points of the increasing relaxation rate according to the size of the droplets as deduced from the SEM images. The dashed lines are guide to the eye.

mode is substantially suppressed by application of an external electric field. The observed behavior is very similar to the features found by DLS studies of conventional PDLCs and other types of confined LC systems. Analogous to these systems we relate the fast mode to intradroplet or intrapore orientational fluctuations, while the slow mode is attributed to orientational diffusion of the preferential director orientation due to randomness and irregularities of the polymer-LC interface [36–39]. In view of this model our results show that in the UV samples the nematic director field $\mathbf{n}(\mathbf{r})$ has a well defined preferential configuration, while in the VIS samples several configurations can be realized with similar probabilities.

Measurements of the dispersion relation of inverse relaxation time $1/\tau_f(\mathbf{q_s})$ provide information on viscoelastic parameters of the LC material within the droplets. For droplet sizes in the range of optical wavelength, which are characteristic of most of the H-PDLC samples, they additionally provide information on the droplet dimensions. A typical result obtained for VIS samples is shown in Fig. 4. At low scattering angles relaxation rate $1/\tau_f$ is independent of q_s and has a value of 5 kHz for both scattering configurations. According to Eq. (2) the dynamic structure factor for $q_s \rightarrow 0$ is predominantly determined by the properties of the optical dielectric tensor fluctuation with the longest possible spatial

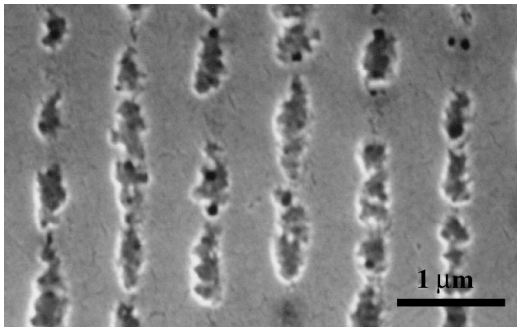

FIG. 5. Scanning electron microscopy (SEM) image of the VIS sample.

periodicity (i. e., by the fundamental eigenmode of director orientational fluctuations). The behavior of this mode is very important for the electro-optic response of the gratings, as its relaxation time determines the so-called "off time," which is the characteristic time to restore the diffraction efficiency after the removal of the external field.

The magnitude of q_s at which $1/\tau_f$ starts to increase by increasing q_s depends on the droplet size and is given by $q_{\min} \sim \pi/d$, where d is characteristic dimension of confinement in the direction of $\mathbf{q_s}$. As evident from Fig. 4 for $\mathbf{q_s} \| \mathbf{K}_g$ this happens at significantly larger value of q_s than for $\mathbf{q_s} \perp \mathbf{K}_g$, which indicates that the droplets are squeezed in the direction of $\mathbf{K}_g$ (Fig. 1). This is in agreement with the structure of these samples as revealed from our SEM study (Fig. 5). According to the SEM images the droplets are oblate ellipsoids of about $250 \times 600 \times 600$ nm^3 in size. In Fig. 4 one can notice that the values of $q_{y,\min}$ and $q_{z,\min}$ corresponding to this size match well the starting points of increasing relaxation rate $1/\tau_f$. This finding is important due to the fact that SEM usually probes morphology of the H-PDLC layer in contact with glass substrates, which in principle might be quite different from the bulk morphology probed by DLS. Besides this, SEM requires fracturing of the sample and removal of the LC, while DLS is practically nondestructive. Our results show that the surface and the bulk morphologies of our VIS H-PDLC gratings are very similar. They also demonstrate that DLS is a convenient alternative method to probe the size and the shape of the LC domains in H-PDLCs.

In this respect we should mention that the above reported result is, however, more of an exception than the rule. It is usually observed that the differences in the surface tension between the glass and the prepolymer syrup give rise to some preferential surface structure, which is typically considerably different from the bulk structure. For our UV-A gratings, for instance, SEM revealed nondroplet structure of the contact layer, while DLS showed that relatively small LC domains of the sizes below 200 nm are present in the bulk. An extensive comparative study of the surface and bulk morphologies for different mixtures will be reported in a separate paper.

To explain the observed value of $1/\tau_f$ at $q_s \rightarrow 0$ one needs to know the orientational fluctuation spectrum in more detail. In the literature, calculations of the normal modes of director fluctuations can be found for planar cells [40], for infinitely long cylindrical pores [41], and for spherical droplets with

radial director profile [42], while to the best of our knowledge no theoretical analysis for spherical droplets with other types of equilibrium structures or for ellipsoidal droplets has been disclosed. It is, however, reasonable to expect that for oblate ellipsoids the behavior is intermediate between the spherical and the planar geometry and to facilitate the analysis we examine the situation of finite cylindrical cavities.

Due to strongly prevailing diffraction for *p*-polarized light we assume that the nematic director field $\mathbf{n}(\mathbf{r})$ is in average pointing along the grating wave vector $\mathbf{K}_g$, i.e., along the symmetry axis of the droplets. The corresponding structure can be described by hybrid boundary conditions, i.e., the anchoring on base planes of the cylindrical cavities is assumed to be homeotropic, while the anchoring on side walls is taken to be planar. The nematic phase is hence confined to the region $-L_d/2<z<L_d/2$ and $0<\rho<R$ (where $\rho=\sqrt{x^2+y^2}$, L_d is the length and R the radius of cylindrical LC domains) and has a homogeneous equilibrium structure given by $\mathbf{n}_0=(0,0,1)$. The orientational fluctuations take place in the *xy* plane and can be expressed as

$$\delta\mathbf{n}(\mathbf{r},\mathbf{t}) = f_x(\rho,\varphi,z,t)\mathbf{e}_x + f_y(\rho,\varphi,z,t)\mathbf{e}_y, \tag{5}$$

where φ denotes azimuthal angle in cylindrical coordinates. For $q_s\rightarrow 0$ the HV scattering is due to the fluctuations of $\delta\varepsilon_{yz}(\mathbf{r},\mathbf{t})$ [Eq. (2)] which are related to $\delta\mathbf{n}(\mathbf{r},\mathbf{t})$ by

$$\delta\varepsilon_{yz}(\mathbf{r},\mathbf{t}) = \varepsilon_a f_y(\rho,\varphi,z,t), \tag{6}$$

where ε_a denotes optical dielectric anisotropy of the LC medium.

Neglecting backflow effects and taking the one elastic constant approximation, the normal fluctuation modes are obtained as solutions of the Helmholz-like equation [40]

$$K\nabla^2\delta\mathbf{n}(\mathbf{r},\mathbf{t}) = \eta(\partial\,\delta\mathbf{n}/\partial t), \tag{7}$$

where K stands for elastic constant and η for effective rotational viscosity of the nematic phase. Consequently f_x and f_y have a form of Bessel functions of the first kind in the radial direction and a form of sinusoidal waves along the z axis. The fundamental eigenmode has the following form:

$$f_{x0}, f_{y0} \propto e^{-t/\tau_0} J_0(k_{\rho 0}\rho)\,\cos(k_{z0}z), \tag{8}$$

with the inverse relaxation time given by

$$\frac{1}{\tau_0} = \frac{K}{\eta}(k_{\rho 0}^2 + k_{z0}^2), \tag{9}$$

where $k_{\rho 0}$ and k_{z0} are determined by boundary conditions [40]. For strong anchoring, i.e., for surface anchoring energy coefficient $W\gg K/R$ and $W\gg K/L_d$, these give $k_{\rho 0}=2.4/R$ and $k_{z0}=\pi/L_d$, while in case of weak anchoring, i.e., for $W\ll K/R$ and $W\ll K/L_d$, they yield $k_{\rho 0}=k_{z0}=0$. From this it follows that for any value of W the relaxation rate of the fundamental mode $1/\tau_0$ is below

$$\frac{1}{\tau_{0,\max}} = \frac{K}{\eta}\left[\left(\frac{2.4}{R}\right)^2 + \left(\frac{\pi}{L_d}\right)^2\right]. \tag{10}$$

In order to calculate the value of $\tau_{0,\max}$ for our samples the viscoelastic parameters of the liquid crystal mixture BL038 used in the VIS gratings were measured by DLS on standard 50 μm thick planarly aligned LC cells [43]. The obtained diffusivities were $K_3/\eta_b=3.0\times10^{-10}$ m^2/s for bend and $K_1/\eta_s=3.5\times10^{-11}$ m^2/s for splay fluctuations, respectively. The twist diffusivity K_2/η_t was not measured, but as it is generally found that $K_2/\eta_t<K_1/\eta_s<K_3/\eta_b$ [44] we take the average viscoelastic constant as $K/\eta\sim\frac{1}{3}(K_3/\eta_b+K_1/\eta_s)=1.1\times10^{-10}$ m^2/s. According to this pure BL038 confined to the cylinders of $L=250$ nm and $2R=600$ nm should have the values of $1/\tau_0$ in the range of 0–25 kHz. Very similar result is expected for other kinds of 3D cavity shapes. Our experimental observation of the relaxation rate of 5 kHz, which is in the lower range of possible values, signifies that LC material phase separated from the polymer network is either very weakly anchored to the polymer surface and/or mixed with other constituents which affect its viscoelastic properties. For the latter case, dissolved parts of polymer chains are particularly important, as their presence is known to drastically increase the effective viscosity of the nematic phase [45–47].

To find out which of the above mentioned effects is most prominent in our samples, the dispersion relation $1/\tau_f(q_s)$ was also analyzed for large values of q_s. This is reasonable only in $\mathbf{q_s}\perp\mathbf{K}_g$ geometry. For $q_s\gg q_{\min}$ again only one eigenmode is expected to predominate the DLS response and a bulklike parabolic dispersion given by the expression

$$\frac{1}{\tau(q_s)} = \frac{K}{\eta}(q_s^2 + k_{z0}^2) \tag{11}$$

should be observed. The best fit of experimental data obtained for $q_s>2q_{y,\min}$ to Eq. (11) is shown as a solid line in Fig. 4 and results in $K/\eta=(0.3\pm0.06)\times10^{-10}$ m^2/s and $k_{z,0}=(0.9\pm0.5)\times10^7$ m^{-1}. The diffusivity of a LC material in the droplets is hence almost four times lower than the diffusivity of a pure BL083, which is attributed to the increased viscosity of a LC medium [45]. This demonstrates that to properly explain the dynamic properties of the H-PDLC gratings, such as switching-on and -off times, etc., it may not be relevant to take viscoelastic parameters of the LC material as used for the mixture, but one needs to measure the properties of a nematogenic material formed in the phase separation process. Since DLS requires no special sample treatment, it is one of the most convenient techniques to perform this task [38].

The obtained value of k_{z0} can be used to calculate the extrapolation length $\lambda_e=K/W$ of the fluctuation modes along the z axis. For $(K/W)\gtrsim L_d$ this parameter corresponds to the depth from the interface at which the amplitude of normal modes drops to zero [43]. For fundamental mode it yields $k_{z0}=\pi/(L_d+2\lambda_e)$ and consequently for our case it follows $\lambda_e=65\pm35$ nm. Taking the values of elastic constants for BL083 $K_3=27.7$ pN, $K_1=13.7$ pN as specified by the producer (EM Industries) and $K\sim\frac{1}{3}(K_3+K_1)=13.8$ pN we then obtain $W=(2.1\pm1.1)\times10^{-4}$ Jm^{-2}, which is consistent with surface anchoring energy measurements in other H-PDLC systems photopolymerized with VIS irradiation [22].

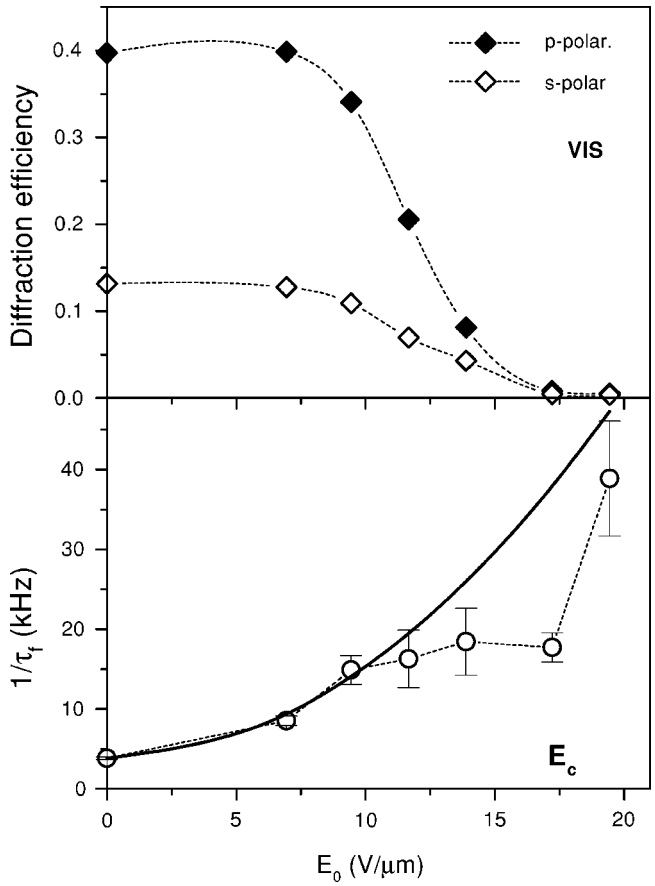

FIG. 6. Diffraction efficiencies and relaxation rate of the fast DLS mode as functions of amplitude of external electric field measured in VIS grating at room temperature. Solid line is a fit to parabolic dispersion for small field amplitudes. The dashed lines are a guide for the eye.

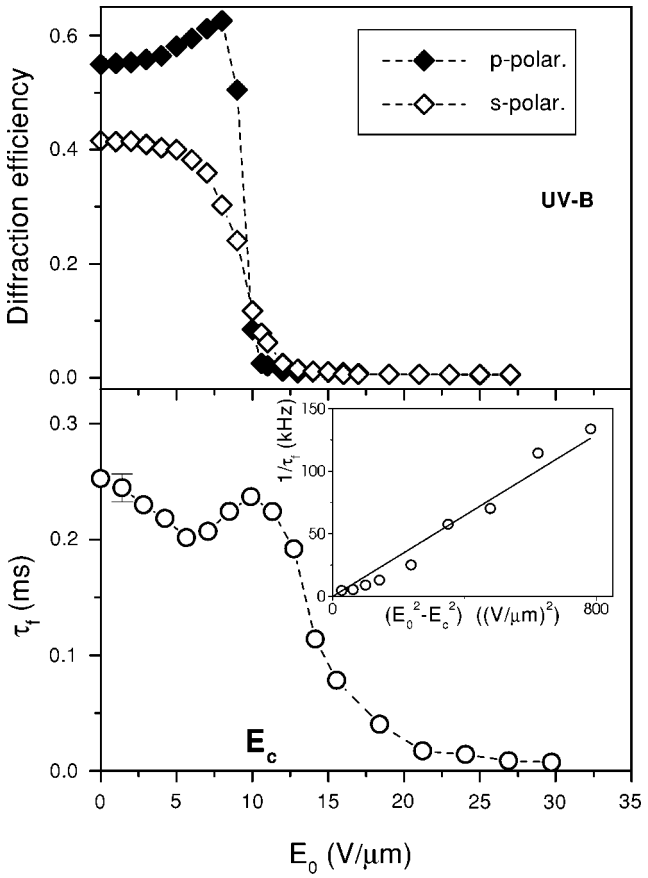

FIG. 7. Diffraction efficiencies and relaxation time of the fast DLS mode as functions of amplitude of external electric field measured in UV-B grating at room temperature. Solid line in the inset is a fit to linear dependence. The dashed lines are a guide for the eye.

The analysis described above is possible only if the LC domain sizes are of the order of optical wavelength or larger. For droplet sizes below optical wavelength, as usually found in reflection gratings, the dispersion as given by Eq. (11) is no longer observed. For that reason the values of K/η and K/W cannot be determined separately, but only their ratio can be found [48].

B. Field induced structural transition

Application of external electric field in the direction parallel to the grating planes $\mathbf{E}=E_0\mathbf{e}_x$ breaks the intrinsic axial symmetry of the nematic director field within the droplets. For our samples, in which $\mathbf{n}(\mathbf{r})$ is on average orthogonal to $\mathbf{E}$, this is expected to cause a slowing down of orientational fluctuations similar to the case of Freedericksz transition in planar nematic cells [49–51]. Figure 6 shows the dependencies of η_d and τ_f as functions of the amplitude of external electric field for a VIS grating. The DLS data were obtained in the $\mathbf{q_s}\perp\mathbf{K}_g$ scattering geometry at $\theta_s=40°$ and correspond to the region in which the scattering due to fundamental mode of director fluctuations is predominant. A significant deviation of $1/\tau_f(E_0)$ from a usual parabolic behavior characteristic for randomly oriented droplet directors is apparent [37].

Figure 7 shows the analogous results achieved for a UV-B grating. This material showed the most pronounced slowing down of relaxation dynamics in the vicinity of some critical field E_c. To demonstrate the effect more clearly we plot the DLS data in the form of $\tau_f(E_0)$ rather than $1/\tau_f(E_0)$. The values of τ_f were obtained in the $\mathbf{q_s}\perp\mathbf{K}_g$ scattering geometry at $\theta_s=60°$ and again fundamental mode prevailed. Below E_c, a nonmonotonous behavior of $\tau_f(E_0)$ takes place, while above E_c the relaxation time decreases with increasing E_0. In the graph for $\eta_d(E_0)$, one can notice that just above E_c there is an interval in which the diffraction efficiency for *s* polarization is significantly larger than for *p* polarization. This is associated with the region in which the droplet directors are already preferentially lying in the *xy* plane, but are not yet fully aligned along the electric field. For that reason the refractive-index mismatch for *s* polarization is larger than for *p* polarization. At even higher fields the structure is close to $\mathbf{n}(\mathbf{r})=(1,0,0)$ and the diffraction efficiency for both polarizations is about the same. All these observations suggest that a Freedericksz-like structural transition from $\mathbf{n}(\mathbf{r})\sim(0,0,1)$ to $\mathbf{n}(\mathbf{r})\sim(1,0,0)$ takes place at $E=E_c$.

Let us again revisit our simple model of cylindrical pores. For $\mathbf{E}=E_0\mathbf{e}_x$ the dynamic equation for the fluctuations becomes

$$K\nabla^2\delta\mathbf{n}(\mathbf{r},\mathbf{t}) + \varepsilon_0\varepsilon_a E_0^2(\mathbf{e}_x\delta\mathbf{n})\mathbf{e}_x = \eta(\partial\,\delta\mathbf{n}/\partial\,t), \qquad (12)$$

and accordingly the relaxation rate of fundamental director fluctuations [Eq. (8)] parallel to the $\mathbf{e}_x$ axis is given by

$$\frac{1}{\tau_{0,x}} = \frac{K}{\eta}\left(k_{\rho 0}^2 + k_{z0}^2 - \frac{\varepsilon_0\varepsilon_a E_0^2}{K}\right) = \frac{\varepsilon_0\varepsilon_a}{\eta}(E_c^2 - E_0^2). \qquad (13)$$

Dielectric interaction destabilizes the equilibrium director configuration $\mathbf{n}_0(\mathbf{r})=(0,0,1)$ and at $E_0=E_c=[K(k_{\rho,0}^2+k_{z,0}^2)/\varepsilon_0\varepsilon_a]^{1/2}$ the fluctuations along $\mathbf{e}_x$ axis are "frozen" and correspondingly the second-order structural transition takes place. Contrary to this, the relaxation rate of fluctuations parallel to the $\mathbf{e}_y$ axis is not influenced by $\mathbf{E}=E_0\mathbf{e}_x$ and remains the same as in the absence of the field [Eq. (9)].

Above the structural transition equilibrium director profile $\mathbf{n}_0(\mathbf{r})$ is no longer orthogonal to the field. This feature modifies its dielectric coupling to the field and as a result for $E_0>E_c$ the effect of the field is that it stabilizes the structure by suppressing the fluctuations. Analogous to Eq. (13) in the vicinity of E_c the response of the critical mode is expected to be governed by $E_0^2-E_c^2$. The best fit of DLS data obtained for $E_0>E_c$ to the relation $1/\tau_f \propto (E_0^2-E_c^2)$ is shown as a solid line in the inset of Fig. 7 and a good agreement is found.

On the contrary, for $E_0<E_c$, the experimentally observed dependence of $\tau_f(E_0)$ is quite different from the behavior associated with Eq. (13). The potential reasons for this are numerous. At selected scattering angles of $\theta_s=40°$ and 60° our DLS experiment probes both: the noncritical $\delta\mathbf{n}\|\mathbf{e}_y$ and the critical fluctuation $\delta\mathbf{n}\|\mathbf{e}_x$ mode, so that the obtained values of τ_f correspond to an average relaxation time determined by relative amplitudes of the two modes [52]. The size of the droplets is not uniform, so that the value of E_c varies from droplet to droplet and a convolution of several critical processes is monitored. The critical phenomena are consequently smoothed. In addition, as shown in our recent paper [27], for a significant part of the droplets the average droplet director is tilted from the $(0,0,1)$ direction, so that they exhibit a noncritical fluctuation dynamics associated to $1/\tau_0 \propto E_0^2$. These "misaligned" droplets are in our opinion the main reason why at low fields τ_f decreases by increasing field and a critical slowing down becomes pronounced only when the scattering from "aligned" droplets start to prevail the DLS response.

C. Temperature induced structural transition

By changing the temperature of H-PDLC gratings an interesting dependence of $\eta_d(T)$ is found, exhibiting notable similarity to the behavior of $\eta(E_0)$ shown in Fig. 7. This is illustrated in Fig. 8, which shows the temperature dependences of η_d and τ_f for a VIS grating. Above some specific temperature the diffraction efficiency for *s* polarization starts to prevail the diffraction efficiency for *p* polarization. This situation is observed up to the nematic-isotropic (N-I) phase transition at which η_s and η_p become nearly the same. The corresponding values of τ_f obtained at $\theta_s=40°$ show that the crossover is associated with the slowing down of the fundamental fluctuation modes, which takes place up to some critical temperature T_c. Above T_c the relaxation time τ_f decreases with increasing temperature.

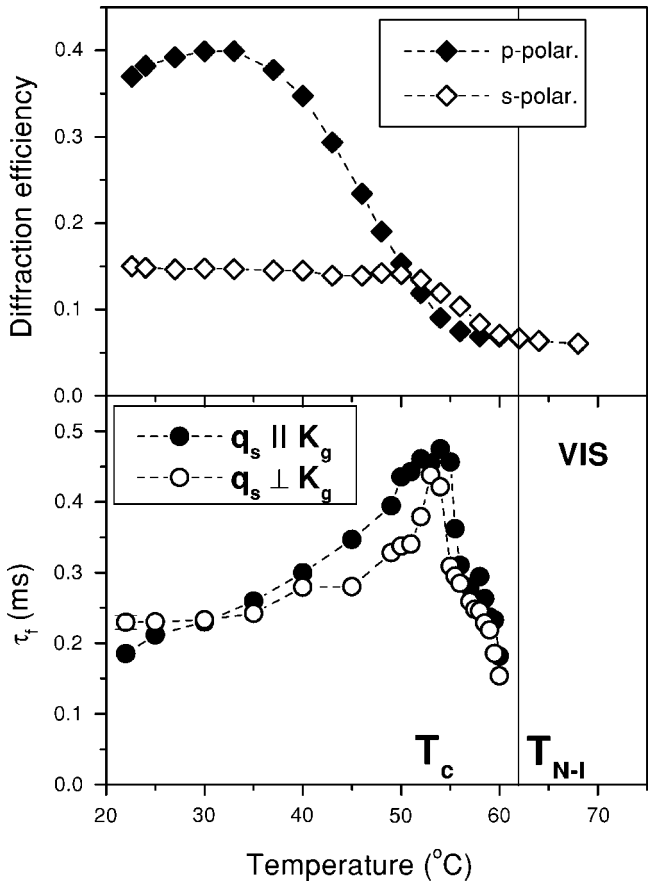

FIG. 8. Temperature dependence of diffraction efficiencies and relaxation time of the fast DLS mode detected in VIS grating in the absence of external field. Vertical line denotes the nematic to isotropic phase transition. The dashed lines are a guide for the eye.

The most pronounced crossover of η_s, with respect to η_p, is found in the UV-A gratings, which at room temperature exhibit an extremely low diffraction for *s* polarization (Fig. 9). This signifies a strong ordering of droplet directors along the $(0,0,1)$ direction. In these samples the relaxation time of director fluctuations τ_f first decreases with increasing temperature and a characteristic slowing down becomes evident at 15°C below T_c. Above T_c a rapid decrease of τ_f is observed, which is nearly linear with increasing temperature. One can also notice that around room temperature the values of τ_f detected in two orthogonal scattering geometries (Fig. 2) are different by a factor of ~1.5. We relate this phenomenon to the anisotropy of viscoelastic parameters of the LC medium. Due to stronger ordering of droplet directors in the UV-A gratings, the anisotropy is much more pronounced than in case of VIS samples.

An additional feature found in both VIS and UV samples is that a strongly nonexponential dynamic mode, which is observed in $g^{(1)}(t)$ at room temperature (Fig. 3), vanishes above T_c. This means that below T_c several configuration of nematic director field can be realized with similar probabilities, while above T_c there exist a well defined preferential

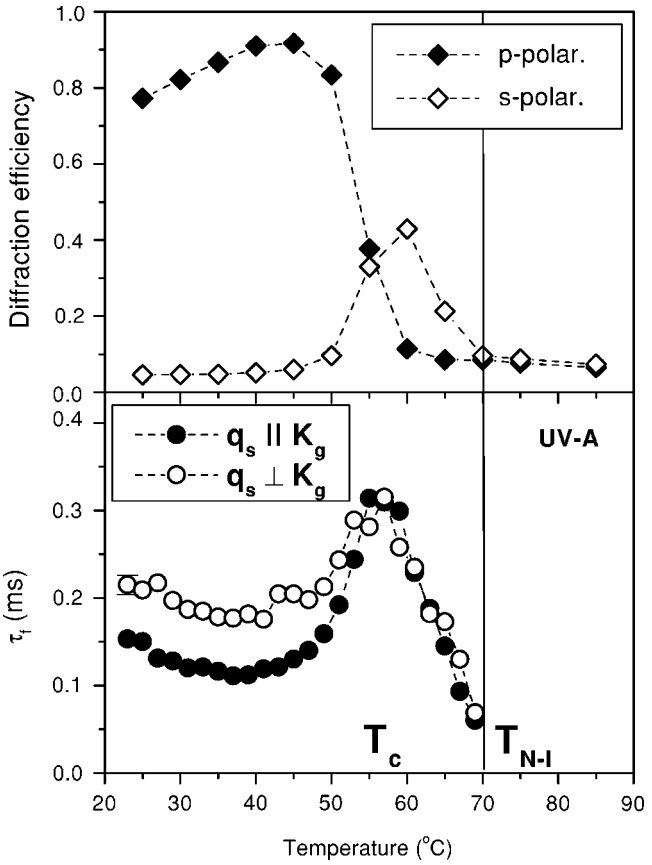

FIG. 9. Temperature dependence of diffraction efficiencies and relaxation time of the fast DLS mode detected in UV-A grating in the absence of external field. Vertical line denotes the nematic to isotropic phase transition. The dashed lines are a guide for the eye.

configuration. This is possible only if the role of polymer-LC interface in fluctuation dynamics is strongly modified at T_c. A strong modification of interface effects can be attributed to a gradual melting of the nematic phase from the surface of the droplets. The polymer-LC interface formed during photopolymerization is usually quite rough [23,24,53] and some dangling parts of polymer chains are probably present in the LC phase. This results in a larger field necessary to cause a considerable reorientation in the interfacial region, as is found in many PDLC systems [54], and results in a local decrease of the N-I transition temperature at the interface. For PDLC droplets of around 10 μm in diameter such a surface induced melting was observed by optical microscopy by Amundson, who found that melting induces structural transition which dramatically affects the electro-optic response of the medium [55].

The reason for reorientation of the droplet director by surface melting in our samples is that the polymer surface prefers a homeotropic alignment of the oblate droplets, while isotropic-nematic liquid crystal interface is known to prefer a tilted, nearly planar director anchoring [56,57]. Consequently at some critical temperature T_c, at which a more or less closed shell of isotropic LC phase is formed between the droplet surface and the central region of the nematic phase, the structural transition of director field from $\mathbf{n}(\mathbf{r}) \sim (0,0,1)$ to $\mathbf{n}(\mathbf{r}) \sim (\cos\varphi, \sin\varphi, 0)$ takes place [58]. This

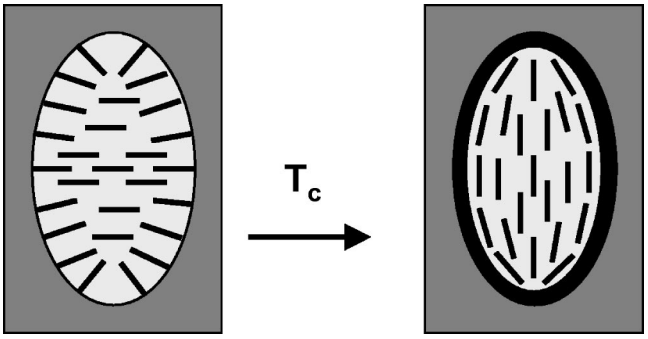

FIG. 10. Schematic illustration of the temperature induced structural transition. The dark region in the right image denotes a layer of the isotropic LC phase formed between the polymer surface and a central region of the nematic phase.

effect is illustrated in Fig. 10. The value of φ associated with the axis of resulting bipolar configuration is determined by the shape and surface topography of a particular droplet. The reorientation causes an increase of refractive-index mismatch for *s* polorization and a decrease of refractive-index mismatch for *p* polarization, so the corresponding diffraction efficiencies are strongly modified with respect to their values at $T < T_c$. A structural transition from homeotropic to quasiplanar anchoring, similar to the one observed in our H-PDLC samples, was recently reported in connection with field induced anchoring breaking [59].

As in the case of electric field induced structural transition the temperature induced structural transition is also associated with critical slowing down of the director fluctuations. However, as reorientation of the droplet director can occur along any direction in the *xy* plane, both $\delta\mathbf{n} \| \mathbf{e}_y$ and $\delta\mathbf{n} \| \mathbf{e}_x$ fundamental modes exhibit a critical behavior of $1/\tau_0$ in the vicinity of T_c and consequently a slowing down detected in DLS experiments is more pronounced than in case of electric field induced transition.

A rapid increase of relaxation rate of fluctuations observed above T_c is attributed to two reasons. First, the increase takes place due to suppression of fluctuations by new boundary conditions. Second, the size of the central regions of nematic phase reduces by increasing temperature [55], so that the wave vectors characterizing the fundamental mode and the associated relaxation rate increase [see Eqs. (10) and (13)]. This takes place until the nematic phase gets completely melted at T_{N-I} and as a result the amplitude of DLS signal is drastically reduced. The observed values of T_{N-I} are considerably lower than the N-I transition temperatures of the pure LC compounds used for the mixture, which again signifies that LC medium forming the droplets is mixed with other constituents used to prepare the grating and hence its material parameters are significantly modified.

IV. CONCLUSIONS

Our measurements show that DLS is a very powerful tool to study the structural and dynamic properties of H-PDLC media. It allows one to determine the size and shape of the LC droplets and to measure viscoelastic and surface anchor-

ing parameters of the LC material phase separated from the polymer matrix. This information is prerequisite in order to optimize the electro-optic performance of the gratings. The technique can in principle be used *in situ*, during the photopolymerization reaction, which provides a way to control the phase separation kinetics, structural morphology, and associated dynamic properties in the course of grating formation.

In contrast to PDLC structures, H-PDLC media exhibit a strong inherent ordering of droplet directors which is related to strongly elongated shape of the LC domains. This property is in general associated with much faster reorientation dynamics as compared to spherical droplets [54,60]. On the other hand, as shown by our experiments, the ordering of droplet directors brings into play the appearance of second-order structural transitions. Therefore, it is necessary to take into account that due to critical slowing down of dynamic processes in the vicinity of structural transitions, the response time of H-PDLCs can also be quite long and strongly dependent on amplitude of external field and on sample temperature.

ACKNOWLEDGMENT

We wish to acknowledge with thanks the joint U.S.-Slovenia grant (Grant No. NSF INT 0306851).

[1] T. J. Trout, J. J. Schmieg, W. J. Gambogi, and A. M. Weber, Adv. Mater. (Weinheim, Ger.) **10**, 1219 (1998).
[2] G. P. Crawford and M. J. Escuti, *Liquid Crystal Display Technology, Encyclopedia of Imaging Science and Technology* (Wiley, New York, 2002).
[3] For a recent review, see, for instance, T. J. Bunning, L. V. Natarjan, V. P. Tondiglia, and R. L. Sutherland, Annu. Rev. Mater. Sci. **30**, 83 (2000).
[4] G. P. Crawford, Opt. Photonics News **14**, 54 (2003).
[5] C. C. Bowley and G. P. Crawford, Appl. Phys. Lett. **76**, 2235 (2000).
[6] T. Kyu, D. Nwabunma, and H.-W. Chiu, Phys. Rev. E **63**, 061802 (2001).
[7] R. L. Sutherland, V. P. Tondiglia, L. V. Natarajan, T. J. Bunning, and W. W. Adams, Appl. Phys. Lett. **64**, 1074 (1994).
[8] R. Jakubiak, T. J. Bunning, R. A. Vaia, L. V. Natarajan, and V. P. Tondiglia, Adv. Mater. (Weinheim, Ger.) **15**, 241 (2003).
[9] K. K. Vardanyan, J. Qi, J. N. Eakin, M. De Sarkar, and G. P. Crawford, Appl. Phys. Lett. **81**, 4736 (2002).
[10] M. J. Escuti, J. Qi, and G. P. Crawford, Opt. Lett. **28**, 522 (2003).
[11] L. H. Domash, Y.-M. Chen, B. Gomatam, C. Gozewski, R. L. Sutherland, L. V. Natarajan, V. P. Tondiglia, T. J. Bunning, and W. W. Adams, Proc. SPIE **2689**, 188 (1996).
[12] H. W. Ren, Y. H. Fan, and S. T. Wu, Appl. Phys. Lett. **83**, 1515 (2003).
[13] L. V. Natarajan, R. L. Sutherland, V. P. Tondiglia, T. J. Bunning, and R. M. Neal, Proc. SPIE **3143**, 182 (1997).
[14] T. G. Fiske, L. D. Silverstein, J. Colegrove, and H. Yuan, SID Digest of Technical Papers **31**, 1134 (2000).
[15] K. Tanaka, K. Kato, and M. Date, Jpn. J. Appl. Phys., Part 2 **38**, L277 (1999).
[16] T. J. Bunning, L. V. Natarajan, V. Tondiglia, R. L. Sutherland, D. L. Vezie, and W. W. Adams, Polymer **36**, 2699 (1995).
[17] T. J. Bunning, L. V. Natarajan, V. P. Tondiglia, and R. L. Sutherland, Polymer **37**, 3147 (1996).
[18] T. J. Bunning, L. V. Natarajan, V. P. Tondiglia, G. Dougherty, and R. L. Sutherland, J. Polym. Sci., Part B: Polym. Phys. **35**, 2825 (1997).
[19] C. C. Bowley, H. J. Yuan, and G. P. Crawford, Mol. Cryst. Liq. Cryst. Sci. Technol., Sect. A **331**, 2069 (1999).
[20] R. T. Pogue, L. V. Natarajan, S. A. Siwecki, V. P. Tondiglia, R. L. Sutherland, and T. J. Bunning, Polymer **41**, 733 (2000).
[21] K. K. Vardanyan, J. Qi, J. N. Eakin, M. De Sarkar, and G. P. Crawford, Appl. Phys. Lett. **81**, 4736 (2002).
[22] M. Escuti, J. Qi, and G. P. Crawford, Appl. Phys. Lett. **83**, 1331 (2003).
[23] M. De Sarkar, J. Qi, and G. P. Crawford, Polymer **43**, 7335 (2002).
[24] M. De Sarkar, N. L. Gill, J. B. Whitehead, and G. P. Crawford, Macromolecules **36**, 630 (2003).
[25] R. L. Sutherland, L. V. Natarajan, V. P. Tondiglia, T. J. Bunning, and W. W. Adams, Proc. SPIE **2152**, 303 (1994).
[26] G. S. Iannacchione, D. Finotello, L. V. Natarajan, R. L. Sutherland, V. P. Tondiglia, T. J. Bunning, and W. W. Adams, Europhys. Lett. **36**, 425 (1996).
[27] M. Jazbinsek, I. D. Olenik, M. Zgonik, A. K. Fontecchio, and G. P. Crawford, J. Appl. Phys. **90**, 3831 (2001).
[28] M. E. Holmes and M. S. Malcuit, Phys. Rev. E **65**, 066603 (2002).
[29] R. L. Sutherland, L. V. Natarajan, V. P. Tondiglia, S. Chandra, C. K. Shepherd, D. M. Brandelik, S. A. Siwecki, and T. J. Bunning, J. Opt. Soc. Am. B **19**, 3004 (2002).
[30] R. L. Sutherland, V. P. Tondiglia, L. V. Natarajan, and T. J. Bunning, Appl. Phys. Lett. **79**, 1420 (2001).
[31] R. L. Sutherland, J. Opt. Soc. Am. B **19**, 2995 (2002).
[32] M. Jazbinšek, I. D. Olenik, M. Zgonik, A. K. Fontecchio, and G. P. Crawford, Mol. Cryst. Liq. Cryst. Sci. Technol., Sect. A **375**, 455 (2002).
[33] B. J. Berne and R. Pecora, *Dynamic Light Scattering* (Dover, Mineola, 2000).
[34] K. S. Schmitz, *An Introduction to Dynamic Light Scattering by Macromolecules* (Academic Press, San Diego, 1990).
[35] *Relaxation in Complex Systems, Proceedings of the Internation Discussion Meeting, Heraklion*, 1990, edited by K. L. Ngai and G. B. Wright (North-Holland, Amsterdam, 1991).
[36] T. Bellini, N. A. Clark, and D. W. Schaefer, Phys. Rev. Lett. **74**, 2740 (1995).
[37] A. Mertelj and M. Čopič, Phys. Rev. E **55**, 504 (1997).
[38] A. Mertelj, L. Spindler, and M. Čopič, Phys. Rev. E **56**, 549 (1997).
[39] M. Čopič and A. Mertelj, Phys. Rev. Lett. **80**, 1449 (1998).
[40] S. Stallinga, M. M. Wittebrood, D. H. Luijendijk, and Th. Rasing, Phys. Rev. E **53**, 6085 (1996).

[41] A. Mertelj and M. Čopič, Phys. Rev. E **61**, 1622 (2000).
[42] J. R. Kelly and P. Palffy-Muhoray, Phys. Rev. E **55**, 4378 (1997).
[43] P. G. de Gennes and J. Prost, *The Physics of Liquid Crystals*, (Clarendon, Oxford, 1993).
[44] W. H. de Jeu, *Physical Properties of Liquid Crystalline Materials* (Gordon and Breach, New York, 1980).
[45] H. J. Coles and M. S. Bancroft, Mol. Cryst. Liq. Cryst. Sci. Technol., Sect. A **237**, 97 (1993).
[46] R. Borsali, U. P. Schroeder, D. Y. Yoon, and R. Pecora, Phys. Rev. E **58**, R2717 (1998).
[47] M. Vilfan, I. Drevenšek Olenik, A. Mertelj, and M. Čopič, Phys. Rev. E **63**, 061709 (2001).
[48] M. Vilfan, A. Mertelj, and M. Čopič, Phys. Rev. E **65**, 041712 (2002).
[49] K. Eidner, M. Lewis, H. K.M. Vithana, and D. L. Johnson, Phys. Rev. A **40**, 6388 (1989).
[50] P. Galatola and M. Rajteri, Phys. Rev. E **49**, 623 (1994).
[51] P. Galatola, J. Phys. II **2**, 1995 (1992).
[52] I. Drevenšek Olenik, M. Jazbinšek, and M. Čopič, Phys. Rev. Lett. **82**, 2103 (1999).
[53] M. Vilfan, B. Zalar, A. K. Fontecchio, M. Vilfan, M. J. Escuti, G. P. Crawford, and S. Žumer, Phys. Rev. E **66**, 021710 (2002).
[54] D. A. Higgins, Adv. Mater. (Weinheim, Ger.) **12**, 251 (2000).
[55] K. Amundson, Phys. Rev. E **53**, 2412 (1996).
[56] B. Jérôme, in *Handbook of Liquid Crystals* edited by D. Demus, J. Goodby, G. W. Gray, H.-W. Spiess, and V. Vill (Wiley-VCH, Weinheim, 1998), Vol. 1, p. 535.
[57] H. Yokoyama, S. Kobayashi, and H. Kamei, Mol. Cryst. Liq. Cryst. **107**, 311 (1984).
[58] R. K. Bharadwaj, T. J. Bunning, and B. L. Farmer, Liq. Cryst. **27**, 591 (2000).
[59] V. S. U. Fazio and L. Komitov, Europhys. Lett. **46**, 38 (1999).
[60] B. G. Wu, J. H. Erdman, and J. W. Doane, Liq. Cryst. **5**, 1453 (1989).